# Preparation of $Cu_2S$ Nanoribbons from Cu(thiocarbamide)Cl·1/2$H_2O$ Complex Nanowires by Solid-state Reaction at Room Temperature without Surfactants

Chunnian Chen,[†,††] Chunling Zhu,[††] Linyun Hao,[††] Yuan Hu,[†] and Zuyao Chen*[††]
[†]*Key laboratory of Fire Science, University of Science & Technology of China (USTC), Hefei, Anhui, 230026, P. R. China*
[††]*Deptartment of Chemistry, USTC, Hefei, Anhui, 230026, P. R. China*

(Received April 19, 2004; CL-040433)

$Cu_2S$ nanoribbons with width of 60–80 nm, length of 200–500 nm, and average thickness of about 8 nm were prepared by means of a simple solid-state reaction at room temperature without surfactants. The product was characterized by various techniques of XRD, XPS, TEM, HRTEM, and UV–vis spectra.

The shape-controllable synthesis of low dimensional metal and semiconductor nanocrystals is of current interest owing to the strong relationship between the physical properties and the shape of nanocrystals.[1] Compared with the cylindrical nanowires, nanoribbons with high aspect ratio of both width and length to thickness are considered a distinctive subgroup of 1-D nanostructure materials. Although several strategies have been developed for the growth of semiconductor nanoribbons, they suffer from the requirements of high temperature, special solvent, or tedious procedures.[2–4] the solid-state reaction at room temperature is a simple, cheaper, and convenient process to prepare low dimensional nanomaterials. More than 40 kinds of nanoparticles have been synthesized by this method.[5]

$Cu_2S$ has been known for a long time as a type of indirect bandgap semiconductor.[6,7] Although its nanorods[6] and nanowires[7] have been synthesized, to our best knowledge, the preparation of low dimensional ribbon-like $Cu_2S$ has not been reported till now. In this paper, we have prepared $Cu_2S$ nanoribbons by grinding at room temperature without any surfactants.

The detailed synthesizing processes are as follows: 1.0-g NaOH and 1.0-g Cu(thiocarbamide)Cl·1/2$H_2O$ precursor, prepared according to the reports of Krunks,[8] are mixed and ground for 2 h. When the mixture becomes black wholly and muddy, 2.0-mL anhydrous ethanol is added. After 1 h grinding, the mixture is washed in an ultrasonic bath with distilled water and anhydrous ethanol, respectively. The product is dried in air at room temperature, and collected for characterization.

The XRD reflections of the sample shown in Figure 1a fit the diffraction patterns of hexagonal $\beta$-$Cu_2S$ (JCPDF No: 26-1116) with the cell parameters $a = 0.3972$ nm and $c = 0.6668$ nm.The broad peaks indicate the small size of the sample. The XRD pattern here is equal to that reported for $Cu_2S$ by Gao et al.[9] The average crystal size of the sample calculated by the Scherrer' equation was about 9.0 nm. The weak peaks between 30° and 40° might be caused by surplus sulfur.[9] It should be noted the base lines are relatively higher, which is generally induced by a high content of heavy metal, which indicates a higher copper content in samples. Quantitative calculations of energy dispersive spectra (EDS) show the ratio of Cu:S to be close to 2:1, which further confirms the results of the XRD patterns. The yield of $Cu_2S$ is near to 95.3%, based on the content of copper.

X-ray photoelectron spectra (XPS) are used to measure the

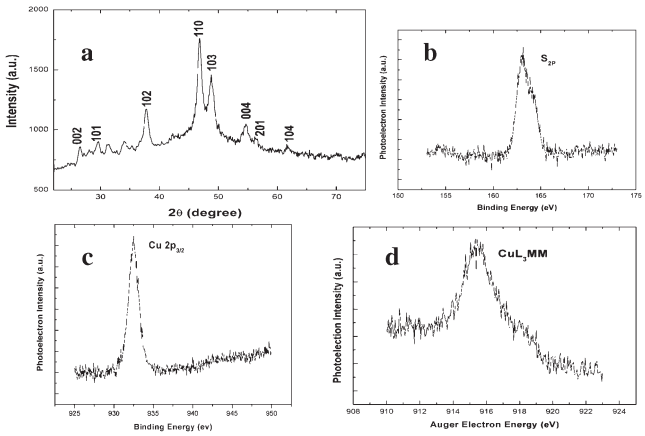


**Figure 1.** a) XRD pattern b) XPS of S 2p c) XPS of Cu 2p d) Cu $L_3$MM Auger spectrum of the as-prepared product $Cu_2S$ sample.

composition of the sample. XPS of S 2p and Cu 2p (Figures 1b and 1c) of the sample show unambiguously the presence of $S^{2-}$, $Cu^+$, or Cu. The distinction between $Cu^+$ and Cu cannot be made from the XPS spectrum in Figure 1c because their binding energy peaks are both at 932.2 eV. However, it is observed that the Auger spectrum shown in Figure 1d shows a peak at 916.9 eV in the Cu $L_3$ MM Auger spectrum, which is a characteristic of Cu (I). The Cu (0) dose not exist in the sample as shown by the absence of characteristic peak of 918.6 eV in the Auger spectrum.[10] According to the XPS and Auger data, the sample consists of only S and Cu. Peak areas of these high-resolution scans are measured and used to calculate the Cu-to-S ratio for the nanocrystals. Quantification gives a Cu-to-S ratio of 2:1.09, close to stoichiometric $Cu_2S$.

The UV–vis spectrum is used to characterize the optical properties of the obtained sample. The absorption spectrum of the sample (Figure 2a) displays a peak at 450 nm and the edge at 650 nm. According to the results reported by Gao et al,[9] the crystal phase of copper sulfide can be handily determined by the absorption spectrum. No other products are formed and the crystal phase of samples is inferred to be pure $Cu_2S$ (chalcocite), in combination with the XRD, UV–vis spectra and XPS results. There is a blue shift compared with the absorption onset of bulk $Cu_2S$ (1022 nm), which indicates a quantum size effect of the sample.

TEM and SAED provide a further insight into the nanostructure of the sample. Figure 2b presents a low-magnification TEM image of the $Cu_2S$ sample. The nanoribbon morphology can be appreciated from the arrows in Figure 2b. The image is darker where the particles overlap compared with the particles isolated, and the optical density of the isolated particles appears homogenous. This overlap phenomenon would not occur for cylindrical

nanowires. It appears that the sample has a relatively uniform width (60–100 nm) and the nanoribbons have many striation contrasts on their observed faces. These are bending contours because of lattice bending in thin samples, where the electronic beams are diffracted, which is fit to Bragg diffraction. These streak lines change in position as the samples are tilted in the TEM measurement. The growth directions for the nanoribbons are determined from the SAED patterns and high-resolution TEM images of individual nanoribbons. The SAED pattern of the ribbon shown in the inset in Figure 2b is recorded with the electron beam along the [010] zone axis (perpendicular to the ribbon), which indicates that the nanoribbons are a single crystal with a growth direction of [002].[9] An HRTEM image shown in Figure 2c further confirms that the single-crystal ribbon grows along the [002] direction (indicated with an arrow). A lot of defects have been seen to distribute uniformly over the nanoribbons in Figure 2c.

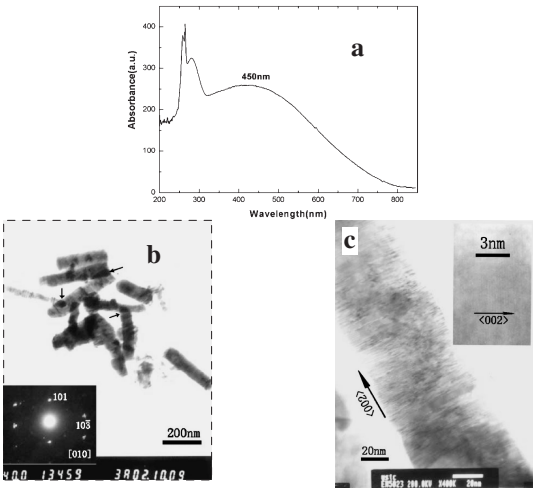


**Figure 2.** a) UV–vis absorption spectrum of the $Cu_2S$ nanoribbons. b) TEM image of $Cu_2S$ nanoribbons. The inset of (b) shows the SAED pattern of the $Cu_2S$ nanoribbons along the [010] axis. c) HRTEM image of the nanoribbons, inset in (c) enlarged image of the selected area in (c), the arrow showing its growth direction [002].

Because of the nature of the nanoribbons, it is difficult to observe their exact thickness by HRTEM. However, the average thickness of the nanoribbons can be calculated according to the bandgap shift because the blue shift is predominantly governed by the sheet thickness.[11]

$$\Delta E_g \approx \frac{h^2}{8\mu_y L_y^2}$$

Here, $\mu_y$ is the reduced effective mass of the exciton, $L_y$ is crystallite dimensions. However, it is difficult to seek the parameter ($\mu_y$) of $Cu_2S$ from handbooks. In work of Gao et al.,[9] the sample IV of $Cu_2S$ nanodisks with thickness of 6 nm presents an absorption peak at 382 nm and the absorption edge at 567 nm ($\Delta E_g = 0.977$ eV). It is deduced from the above Eq: for the different thickness of $Cu_2S$ nanocrystal, $\Delta E_g \cdot L_y^2$ is a constant. Here, $\Delta E_g = 0.64$ eV. So the calculated average thickness of $Cu_2S$ nanoribbons is about 8 nm, which is in good agreement with the average particle size obtained from XRD analysis. For 2-D nanocrystallites, the size calculated by the Scherrer' equation mainly indicates its thickness.

Now we come to investigate the formation mechanism of $Cu_2S$ nanoribbons. It is well known that in basic aqueous solution the $S^{2-}$ ions are generated by hydrolysis of thiocarbamide:

$$NH_2CSNH_2 + 2OH^- \rightarrow S^{2-} + NH_2CN + 2H_2O$$

When NaOH and the Cu(thiocarbamide)$Cl \cdot 1/2H_2O$ complex are mixed and ground in mortar box, owing to deliquescent of NaOH, the high saturated concentration $OH^-$ ions will quickly react to thiocarbamide of Cu(thiocarbamide)$Cl \cdot 1/2H_2O$ complex, which causes the decomposition of the chelate complex. Then, $Cu^+$ ions will react with $S^{2-}$ ions and the $Cu_2S$ is in situ produced.

**Figure 3.** SEM image of wire-like Cu(thiocarbamide)$Cl \cdot 1/2H_2O$ complex.

In SEM image of Cu(thiocarbamide)$Cl \cdot 1/2H_2O$ complex nanowires shown in Figure 3, the complex nanowires with diameters of about 100 nm and lengths of dozens of microns are observed. Some thin precursor nanowires aggregate into bundle-shaped wires. On the basis of above facts, the formation of nanoribbons may be related to the template effects of complex nanowires together with the nature characteristics of $Cu_2S$ crystal growth.[9] Although the exact transformation mechanism from the complex nanowires to $Cu_2S$ nanoribbons is still not clear, the whole process is similar to $Ag_2Se$ nanowires synthesized templating against nanowires of trigonal Se.[12]

In summary, $Cu_2S$ nanoribbons with width of 60–80 nm, length of 200–500 nm and average thickness of about 8 nm are prepared from Cu(thiocarbamide)$Cl \cdot 1/2H_2O$ complex nanowires by a simple solid-state reaction without surfactants and the possible growth mechanism is discussed. The nanoribbons might find application in nanoscaled photoelectronic and semiconductor devices in future.

**References**

1 Z. L. Wang, *Adv. Mater.*, **15**, 432 (2003).
2 X. Duan, C. Niu, V. Sahi, J. Chen, J. W. Parce, S. Empedocles, and J. L. Goldman, *Nature*, **425**, 274 (2003).
3 J. T. Sampanthar and H. C. Zeng, *J. Am. Chem. Soc.*, **124**, 6668 (2002).
4 W. Shi, H. Peng, N. Wang, C. P. Li, L. Xu, C. S. Lee, R. Kalish, and S.-T. Lee, *J. Am Chem. Soc.*, **123**, 11095 (2001).
5 C. F. Jin, X. Yuan, W. W. Ge, J. M. Hong, and X. Q. Xin, *Nanotechnology*, **14**, 667 (2003).
6 T. H. Larsen, M. Sigman, A. Ghezelbash, R. C. Doty, and B. A. Korgel, *J. Am Chem. Soc.*, **125**, 5638 (2003).
7 S. Wang, S. Yang, Z. R. Dai, and Z. L. Wang, *Phys. Chem. Chem. Phys.*, **3**, 3750 (2001).
8 M. Krunks, T. Leskela, R. Mannonen, et al., *J. Therm. Anal. Calorim.*, **53**, 355 (1998).
9 P. Zhang and L. Gao, *J. Mater. Chem.*, **13**, 2007 (2003).
10 S. H. Wang and S. H. Yang, *Mater. Sci. Eng., C*, **16**, 37 (2001).
11 S. H. Yu and M. Yoshimura, *Adv. Mater.*, **14**, 296 (2002).
12 B. Gates, Y. Wu, Y. Yin, P. Yang, and Y. Xia, *J. Am. Chem. Soc.*, **123**, 11500 (2001).

Published on the web (Advance View) June 21, 2004; DOI 10.1246/cl.2004.898